Supplement of Geosci. Model Dev., 19, 4601–4631, 2026
https://doi.org/10.5194/gmd-19-4601-2026-supplement

Geoscientific Model Development
Open Access
EGU

Supplement of

S2AS v1.0 and 2D polarity–volatility lumping framework v1.0: automated compound classification and scalable lumping for organic aerosol modelling

Dalrin Ampritta Amaladhasan et al.

Correspondence to: Andreas Zuend (andreas.zuend@mcgill.ca)

S1 Activity coefficients of binary solutions

The activity coefficient ratio (ACR) is calculated by comparing a solute's activity coefficients in two solvent environments, as predicted by the AIOMFAC model from the binary mixtures containing 0.01 mass fractions of solute. This approach provides a computationally efficient method to characterize the behaviour of organic components across a wide range of polarities. The use of water and 1,2-hexanediol as reference solvents establishes a robust basis for this characterization. Water represents a highly polar solution environment typical of aqueous aerosol phases, while 1,2-hexanediol serves as a proxy for moderately oxidized organic aerosol components that would preferentially partition into an organic-rich phase in the presence of liquid-liquid phase separation (LLPS). This binary solution setup allows for a rapid calculation of ACR values for the numerous organic components from near-explicit mechanism simulations or other rich data sources. The relatively inexpensive binary solution computations with AIOMFAC are indicative of the expected partitioning preferences of organics in atmospheric aerosols without the computational cost of multicomponent mixture calculations.

S2 Volatility in terms of saturation concentration and related secondary volatility axis approximation

The pure-component liquid-state saturation concentration, C_j°, or the effective saturation concentration, denoted C_j^*, can be used alternatively as volatility axis. Note that C_j° and C_j^* are equivalent in case of pure components (Zuend and Seinfeld, 2012) and are commonly used choices in many applications of VBS frameworks. Our 2D polarity–volatility framework and associated code provide both pure-component liquid-state saturation vapour pressure and pure-component liquid-state saturation vapour concentration at the system's temperature in the output files and as options for plotting the volatility axis. For individual compounds of known molar masses, the conversion between p_j° and C_j° is straightforward, refer to Eq. (2) of the main text and the variable units used there.

Figure S1 shows the relationships between molar mass, p_j°, and C_j° for the components of the toluene-derived and α-pinene-derived systems of gas-phase reaction products. For the generation of the upper horizontal (x-axis) shown in several figures of the main text, as well as Fig. S1, a linear relationship between molar mass and saturation vapour pressure was assumed to account for the typical increase in compound molar masses towards lower saturation vapour pressures. For each system, an optimized linear fit of the form $M_j/[\mathrm{g\,mol^{-1}}] = a \cdot \log_{10}\left(p_j^\circ/[\mathrm{Pa}]\right) + b$ was generated. The resulting slope and intercept coefficients (a, b) are listed in Fig. S1a,b. Intercept coefficient b denotes the optimized molar mass at $p_j^\circ = 1$ Pa. The linear function was then applied in Eq. (2) to convert the lowest and highest p° values from the lower (main) x-axis into aligned lowest and highest C° values on the upper x-axis, with even log-scale spacing in between. Therefore, the upper x-axes of such figures indicate an approximate (but not precise) C_j° coordinate of a compound. Panels (c) and (d) of Fig. S1 show the exact relationships of individual components' p_j° and C_j°. These panels further show that, given the large range of volatilities covered, the mapping between the two volatility axes is quasi-linear on log–log scale. A rough conversion estimate is that C_j° values are about five orders of magnitude larger than corresponding p_j°.

The accompanying code, specifically the program in"CustomizedPlots_Dislin" as part of the 2D_Polarity_Volatility_lumping repository, can be used to generate figures such as those shown in Fig. S1, including the linear fits, as well as Figs. 7–12 of the main text (from 2D lumping output for any system of interest). Refer to the *Code and data availability* section of the main text for references to the pertinent code repositories.

S3 Example: SOA mass concentrations calculated using lumped surrogates

The pure-component properties calculated by the S2AS and vapour pressure tools and the lumped mass concentrations obtained for the selected surrogate components can be used by the AIOMFAC-based equilibrium partitioning model to generate the secondary organic aerosol (SOA) prediction of the system. Figure S2 illustrates the predicted SOA mass concentrations as a function of water activity (i.e. equilibrium relative humidity) for the toluene SOA system. The water content itself is not shown in this figure. In this example, the surrogate components were selected via the grid cell mass-weighted medoid method on a 10×5 grid, with ACR as the polarity axis metric. This selection method emphasizes the influence of both the component positions in the 2D grid space and their relative mass contributions. Figure S2a shows that most of the gas-phase mass concentration is due to the special high-volatility surrogate. Panels (b) and (c) show the equilibrium compositions of the liquid phases – with two liquid phases coexisting here only at the highest water activity levels. Note that only the first (top) 30 organic surrogate components are shown in the legend. For this toluene-derived SOA case, the relatively low hygroscopicity is evident from the weak dependence of the condensed-phase mass concentration on the water activity.

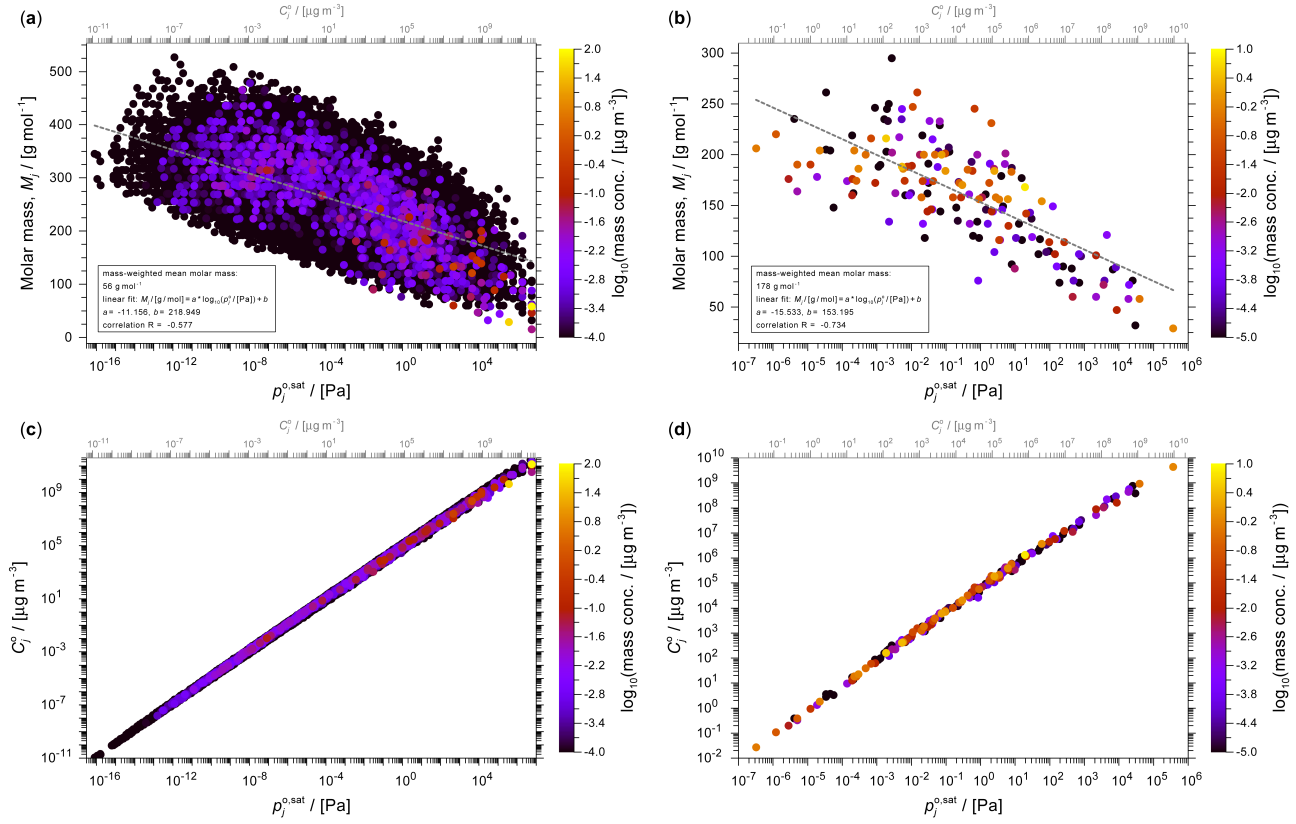

Figure S1. Relationships between molar mass and saturation vapour pressure (a, b) and between component saturation vapour concentration and saturation vapour pressure at $T = 298.15$ K. Panels (a) and (c) for the toluene-derived and panels (b) and (d) for α-pinene-derived systems of gas-phase reaction products. The linear fit in (a, b) is used in the conversion from the lower to upper x-axes in these and related figures.

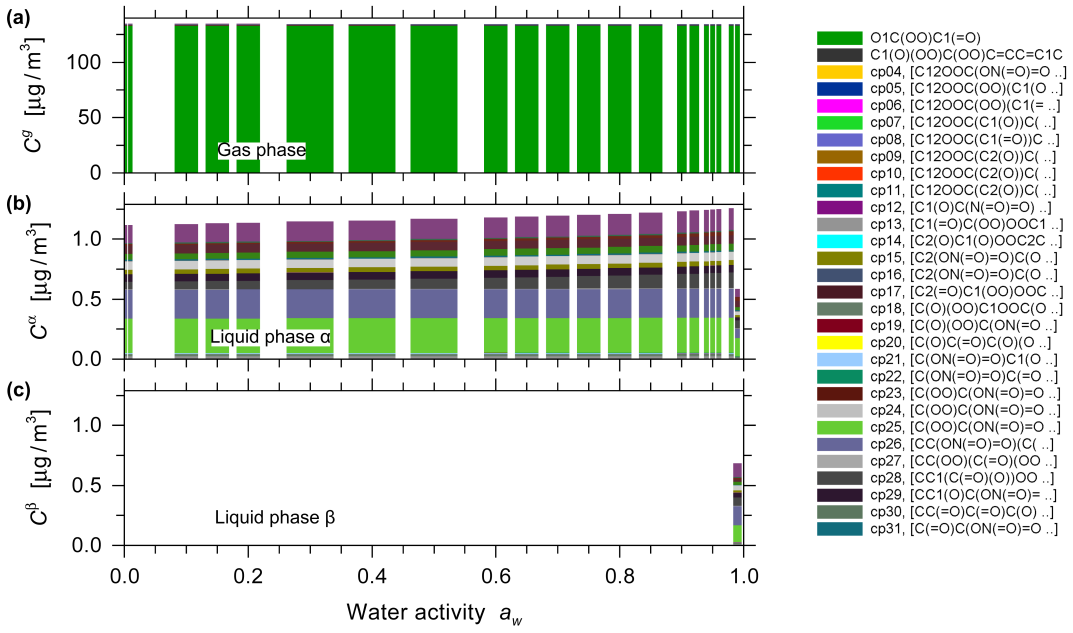

Figure S2. Predicted speciated gas phase (a) and liquid phase (b,c) SOA mass concentrations for the toluene SOA system (water content not shown). The shown surrogate species (legend limited to top 30) were obtained from the 2D lumping framework by means of the mass-weighted medoid surrogate selection method with a 10×5 grid resolution. Liquid–liquid phase separation was predicted to occur at high water activity, where amounts from panels (b) and (c) contribute to the total non-water aerosol mass.

Table S1. Initial precursor and oxidant concentrations as well as the MCM v3.3.1 (AtChem) simulation conditions used for the α-pinene ozonolysis system.

Species	Concentration ($\mathrm{molec\,cm^{-3}}$)
α-pinene	1.23×10^{17}
O_3	2.46×10^{12}
NO	4.43×10^{8}
NO_2	5.90×10^{8}
CO	4.92×10^{12}
H_2	1.23×10^{13}
H_2O	3.00×10^{17}
Temperature	298.15 K
Pressure	1013.25 hPa (1 atm)
Simulation duration	2.8 hours

Table S2. Initial precursor and oxidant concentrations as well as GECKO-A model simulation conditions for the toluene system.

Species	Concentration ($\mathrm{molec\,cm^{-3}}$)
Toluene	2.75×10^{11}
OH	5.11×10^{6}
HO_2	8.41×10^{7}
O_3	1.00×10^{12}
H_2O_2	2.22×10^{9}
NO_2	3.58×10^{11}
NO	1.42×10^{11}
NO_3	3.12×10^{6}
Temperature	298.15 K
Pressure	1013.25 hPa (1 atm)
Simulation duration	24 hours
Timestep size	5 minutes

Table S3. Comparison of predicted SOA mass concentrations and hygroscopicity parameter κ at 298 K for different surrogate selection methods and polarity metrics across four grid resolutions. Data shown are for the α-pinene system.

Surrogate selection	y-axis	4×2		6×3		8×4		10×5	
		SOA ($\mu\mathrm{g\,m^{-3}}$)	κ (–)	SOA ($\mu\mathrm{g\,m^{-3}}$)	κ (–)	SOA ($\mu\mathrm{g\,m^{-3}}$)	κ (–)	SOA ($\mu\mathrm{g\,m^{-3}}$)	κ (–)
Midpoint	$\log_{10}\left[\gamma_{j,\mathrm{hex}}^{(x)}/\gamma_{j,\mathrm{w}}^{(x)}\right]$	1.728	0.042	1.148	0.051	1.584	0.045	1.874	0.040
Medoid		1.613	0.051	1.162	0.049	1.170	0.047	1.834	0.041
Weighted medoid		1.234	0.045	1.586	0.043	1.600	0.043	1.624	0.043
Weighted k-means		1.581	0.042	1.560	0.042	1.544	0.043	1.549	0.044
Midpoint	O:C	2.350	0.076	1.608	0.050	1.856	0.052	1.953	0.045
Medoid		1.451	0.082	1.669	0.061	1.637	0.060	2.209	0.050
Weighted medoid		1.582	0.049	1.845	0.044	1.671	0.050	1.665	0.051
Weighted k-means		1.629	0.050	1.595	0.042	1.536	0.043	1.548	0.044
Midpoint	$\overline{\mathrm{OS}}_{\mathrm{C}}$	2.656	0.059	1.702	0.055	1.932	0.041	1.565	0.041
Medoid		1.569	0.058	1.148	0.045	1.781	0.053	1.578	0.041
Weighted medoid		1.182	0.049	1.542	0.042	1.534	0.041	1.596	0.040
Weighted k-means		1.570	0.040	1.557	0.041	1.563	0.042	1.559	0.043

Table S4. Comparison of predicted SOA mass concentrations and hygroscopicity parameter κ at 298 K for different surrogate selection methods and polarity metrics across five grid resolutions. Data shown are for the toluene-derived SOA system.

Surrogate selection	y-axis	4×2		6×3		8×4		10×5		25×10	
		SOA ($\mu g\,m^{-3}$)	κ (–)	SOA ($\mu g\,m^{-3}$)	κ (–)	SOA ($\mu g\,m^{-3}$)	κ (–)	SOA ($\mu g\,m^{-3}$)	κ (–)	SOA ($\mu g\,m^{-3}$)	κ (–)
Midpoint	$\log_{10}\left[\gamma_{j,\mathrm{hex}}^{(x)}/\gamma_{j,\mathrm{w}}^{(x)}\right]$	1.219	0.043	1.130	0.031	1.239	0.054	1.175	0.034	1.201	0.041
Medoid		1.256	0.039	1.103	0.062	1.179	0.054	1.168	0.031	1.194	0.045
Weighted medoid		1.300	0.047	1.234	0.065	1.184	0.045	1.188	0.040	1.202	0.038
Weighted k-means		1.230	0.030	1.188	0.039	1.205	0.039	1.210	0.037	1.161	0.043
Midpoint	O:C	1.307	0.103	1.038	0.059	1.176	0.032	1.136	0.046	1.131	0.024
Medoid		1.239	0.098	1.157	0.047	1.256	0.028	1.106	0.049	1.135	0.035
Weighted medoid		1.263	0.062	1.184	0.046	1.213	0.064	1.211	0.060	1.152	0.043
Weighted k-means		1.188	0.035	1.163	0.062	1.104	0.031	1.113	0.038	1.181	0.038
Midpoint	$\overline{\mathrm{OS}}_{\mathrm{C}}$	1.278	0.028	1.083	0.063	1.252	0.035	1.154	0.050	1.220	0.055
Medoid		1.140	0.029	1.112	0.052	1.249	0.081	1.165	0.032	1.221	0.048
Weighted medoid		1.293	0.033	1.151	0.040	1.151	0.024	1.140	0.025	1.234	0.049
Weighted k-means		1.202	0.072	1.185	0.035	1.160	0.055	1.195	0.053	1.185	0.047

Table S5. Tabulated surrogate component coordinates (first two columns from the left), other component properties and the lumped total mass concentration (gas plus particle phase) represented by the component (last column) for the toluene-derived system (k-means, 10×5 resolution case; corresponding to Fig. 8b).

p° (Pa)	ACR	M (kg mol^{-1})	C° (µg m^{-3})	O:C	Mass conc. [a] (µg m^{-3})
1.884×10^{6}	4.387×10^{-1}	1.051×10^{-1}	7.986×10^{10}	1.333×10^{0}	1.332×10^{2}
6.666×10^{-6}	3.117×10^{0}	2.671×10^{-1}	7.182×10^{-1}	1.833×10^{0}	4.784×10^{-2}
6.970×10^{-9}	3.333×10^{0}	2.681×10^{-1}	7.539×10^{-4}	1.429×10^{0}	7.528×10^{-2}
3.999×10^{-10}	1.043×10^{0}	2.851×10^{-1}	4.600×10^{-5}	1.571×10^{0}	9.281×10^{-2}
3.547×10^{-6}	7.615×10^{-3}	3.571×10^{-1}	5.110×10^{-1}	2.000×10^{0}	5.595×10^{-3}
4.471×10^{-2}	4.990×10^{-1}	1.581×10^{-1}	2.852×10^{3}	5.714×10^{-1}	7.248×10^{-2}
6.429×10^{-4}	1.440×10^{-1}	2.921×10^{-1}	7.574×10^{1}	1.250×10^{0}	2.247×10^{-2}
1.647×10^{-11}	1.061×10^{1}	2.561×10^{-1}	1.702×10^{-6}	1.833×10^{0}	1.126×10^{-2}
1.131×10^{-1}	3.431×10^{-2}	1.781×10^{-1}	8.123×10^{3}	1.200×10^{0}	1.879×10^{-1}
7.501×10^{-3}	8.439×10^{-2}	3.541×10^{-1}	1.071×10^{3}	1.625×10^{0}	1.526×10^{-2}
4.928×10^{-1}	3.262×10^{-1}	2.481×10^{-1}	4.932×10^{4}	1.125×10^{0}	5.180×10^{-2}
1.144×10^{-7}	1.238×10^{0}	2.201×10^{-1}	1.016×10^{-2}	1.143×10^{0}	6.789×10^{-2}
2.159×10^{-3}	6.970×10^{-1}	3.101×10^{-1}	2.701×10^{2}	1.500×10^{0}	3.375×10^{-2}
1.887×10^{-8}	1.068×10^{1}	2.721×10^{-1}	2.071×10^{-3}	1.833×10^{0}	6.380×10^{-2}
8.031×10^{-7}	1.792×10^{0}	2.551×10^{-1}	8.264×10^{-2}	1.667×10^{0}	6.156×10^{-2}
7.435×10^{-7}	1.141×10^{1}	2.970×10^{-1}	8.909×10^{-2}	1.571×10^{0}	3.165×10^{-2}
4.555×10^{-8}	1.934×10^{-1}	3.111×10^{-1}	5.717×10^{-3}	1.500×10^{0}	6.611×10^{-2}
2.386×10^{-5}	1.500×10^{-1}	2.681×10^{-1}	2.581×10^{0}	1.667×10^{0}	2.223×10^{-2}
5.042×10^{-10}	8.077×10^{0}	3.172×10^{-1}	6.451×10^{-5}	1.857×10^{0}	2.243×10^{-2}
3.999×10^{-10}	4.136×10^{-1}	2.861×10^{-1}	4.616×10^{-5}	1.571×10^{0}	3.470×10^{-2}
2.574×10^{-12}	2.580×10^{-1}	2.531×10^{-1}	2.628×10^{-7}	1.429×10^{0}	1.146×10^{-2}
4.469×10^{-7}	6.315×10^{-2}	2.852×10^{-1}	5.141×10^{-2}	1.571×10^{0}	6.830×10^{-3}
1.169×10^{-11}	3.785×10^{-2}	3.441×10^{-1}	1.623×10^{-6}	2.000×10^{0}	1.750×10^{-3}
2.029×10^{-2}	2.072×10^{-1}	2.071×10^{-1}	1.695×10^{3}	1.167×10^{0}	8.547×10^{-2}
2.582×10^{-4}	8.317×10^{0}	2.360×10^{-1}	2.459×10^{1}	1.500×10^{0}	1.262×10^{-2}
1.061×10^{-1}	1.368×10^{0}	2.201×10^{-1}	9.422×10^{3}	1.143×10^{0}	2.109×10^{-1}
1.866×10^{-3}	3.215×10^{-2}	3.251×10^{-1}	2.448×10^{2}	1.500×10^{0}	9.851×10^{-3}
7.229×10^{-5}	1.874×10^{0}	2.841×10^{-1}	8.285×10^{0}	1.571×10^{0}	1.032×10^{-1}
2.830×10^{-6}	3.081×10^{1}	2.810×10^{-1}	3.208×10^{-1}	1.571×10^{0}	2.251×10^{-2}
4.002×10^{-6}	5.135×10^{-1}	3.741×10^{-1}	6.040×10^{-1}	2.143×10^{0}	3.883×10^{-2}
8.384×10^{-8}	4.581×10^{0}	3.410×10^{-1}	1.153×10^{-2}	2.000×10^{0}	1.336×10^{-1}
1.848×10^{-5}	7.362×10^{0}	2.571×10^{-1}	1.917×10^{0}	2.000×10^{0}	6.374×10^{-2}
3.990×10^{-3}	5.264×10^{0}	1.820×10^{-1}	2.930×10^{2}	2.667×10^{0}	8.406×10^{-2}
3.923×10^{-13}	8.308×10^{0}	2.581×10^{-1}	4.084×10^{-8}	1.833×10^{0}	2.401×10^{-3}
2.090×10^{-10}	2.436×10^{0}	3.031×10^{-1}	2.555×10^{-5}	2.167×10^{0}	5.039×10^{-2}
1.175×10^{-8}	5.234×10^{-1}	3.691×10^{-1}	1.749×10^{-3}	1.875×10^{0}	5.454×10^{-2}
9.875×10^{-13}	1.899×10^{0}	2.981×10^{-1}	1.188×10^{-7}	1.500×10^{0}	1.298×10^{-2}

Table S5. Continued.

p° (Pa)	ACR	M (kg mol^{-1})	C° (µg m^{-3})	O:C	Mass conc. [a] (µg m^{-3})
6.211×10^{-4}	3.208×10^{1}	3.141×10^{-1}	7.870×10^{1}	1.857×10^{0}	4.071×10^{-2}
7.860×10^{-3}	1.743×10^{1}	2.511×10^{-1}	7.961×10^{2}	1.429×10^{0}	2.358×10^{-2}
6.935×10^{-9}	3.373×10^{1}	3.601×10^{-1}	1.007×10^{-3}	2.143×10^{0}	2.037×10^{-2}
8.311×10^{-7}	3.818×10^{0}	2.841×10^{-1}	9.524×10^{-2}	1.571×10^{0}	3.658×10^{-2}
7.155×10^{-5}	6.053×10^{-1}	2.881×10^{-1}	8.315×10^{0}	2.400×10^{0}	4.361×10^{-2}
2.076×10^{-11}	6.419×10^{-1}	4.391×10^{-1}	3.678×10^{-6}	2.714×10^{0}	2.823×10^{-2}
5.841×10^{-9}	1.293×10^{0}	3.741×10^{-1}	8.815×10^{-4}	2.143×10^{0}	6.882×10^{-2}
8.773×10^{-2}	3.780×10^{0}	2.691×10^{-1}	9.522×10^{3}	1.833×10^{0}	6.125×10^{-2}
2.054×10^{-1}	9.645×10^{-2}	3.251×10^{-1}	2.693×10^{4}	1.857×10^{0}	6.763×10^{-2}
2.270×10^{-2}	6.667×10^{0}	2.360×10^{-1}	2.161×10^{3}	1.500×10^{0}	8.335×10^{-2}
1.076×10^{-1}	7.721×10^{0}	2.831×10^{-1}	1.228×10^{4}	1.571×10^{0}	6.672×10^{-2}
5.697×10^{-3}	1.550×10^{0}	2.971×10^{-1}	6.828×10^{2}	1.571×10^{0}	5.177×10^{-2}
1.144×10^{-5}	1.074×10^{0}	3.301×10^{-1}	1.524×10^{0}	2.333×10^{0}	2.703×10^{-2}

Table S6. Tabulated surrogate component coordinates (first two columns from the left), other component properties and the lumped total mass concentration (gas plus particle phase) represented by the component (last column) for the α-pinene-derived system (k-means, 10×5 resolution case; corresponding to Fig. 10b).

p° (Pa)	ACR	M (kg mol^{-1})	C° (µg m^{-3})	O:C	Mass conc. [a] (µg m^{-3})
4.250×10^{-1}	1.242×10^{-2}	1.852×10^{-1}	3.175×10^{4}	3.000×10^{-1}	2.458×10^{-1}
7.514×10^{-3}	3.581×10^{-1}	1.881×10^{-1}	5.703×10^{2}	4.444×10^{-1}	3.039×10^{-2}
2.730×10^{-1}	1.517×10^{0}	1.581×10^{-1}	1.740×10^{4}	5.714×10^{-1}	2.209×10^{-2}
3.689×10^{-2}	5.785×10^{0}	1.461×10^{-1}	2.173×10^{3}	6.667×10^{-1}	1.132×10^{-2}
3.226×10^{-7}	3.165×10^{-1}	2.061×10^{-1}	2.682×10^{-2}	7.500×10^{-1}	4.683×10^{-1}
3.424×10^{-3}	2.034×10^{0}	1.621×10^{-1}	2.238×10^{2}	8.333×10^{-1}	1.999×10^{-3}
1.950×10^{-2}	3.046×10^{-2}	1.582×10^{-1}	1.244×10^{3}	3.750×10^{-1}	2.808×10^{-1}
1.845×10^{-3}	3.173×10^{-2}	2.161×10^{-1}	1.608×10^{2}	5.000×10^{-1}	3.636×10^{0}
2.057×10^{1}	5.681×10^{-3}	1.422×10^{-1}	1.180×10^{6}	2.500×10^{-1}	1.267×10^{1}
2.102×10^{-2}	5.309×10^{-1}	1.741×10^{-1}	1.476×10^{3}	7.143×10^{-1}	4.750×10^{-2}
4.289×10^{-2}	5.606×10^{-3}	1.742×10^{-1}	3.014×10^{3}	5.000×10^{-1}	8.716×10^{-2}
4.792×10^{-4}	2.637×10^{-2}	2.002×10^{-1}	3.870×10^{1}	4.000×10^{-1}	2.997×10^{-1}
2.280×10^{-2}	4.999×10^{-3}	2.002×10^{-1}	1.841×10^{3}	4.000×10^{-1}	4.176×10^{-1}
4.977×10^{-6}	5.301×10^{0}	1.641×10^{-1}	3.294×10^{-1}	1.200×10^{0}	1.822×10^{-3}
4.747×10^{-2}	9.340×10^{-2}	2.001×10^{-1}	3.833×10^{3}	4.000×10^{-1}	2.871×10^{-1}
8.974×10^{-1}	1.869×10^{-2}	1.561×10^{-1}	5.652×10^{4}	3.750×10^{-1}	2.477×10^{-1}
1.087×10^{-2}	7.781×10^{-3}	2.472×10^{-1}	1.084×10^{3}	7.778×10^{-1}	1.570×10^{-1}
2.967×10^{-4}	2.847×10^{-2}	1.862×10^{-1}	2.228×10^{1}	4.444×10^{-1}	6.731×10^{-1}
2.793×10^{-6}	2.143×10^{-1}	1.761×10^{-1}	1.985×10^{-1}	7.143×10^{-1}	7.976×10^{-3}
6.709×10^{-1}	2.998×10^{-3}	2.452×10^{-1}	6.636×10^{4}	6.000×10^{-1}	4.021×10^{-2}
5.018×10^{-6}	4.994×10^{-2}	1.902×10^{-1}	3.850×10^{-1}	6.250×10^{-1}	1.700×10^{-1}
2.937×10^{-1}	7.914×10^{-3}	1.702×10^{-1}	2.016×10^{4}	3.333×10^{-1}	9.273×10^{-1}
1.210×10^{-6}	2.939×10^{-1}	2.201×10^{-1}	1.074×10^{-1}	6.667×10^{-1}	1.509×10^{-1}
2.222×10^{-5}	4.636×10^{-2}	2.042×10^{-1}	1.830×10^{0}	5.556×10^{-1}	5.590×10^{-1}
2.247×10^{-4}	1.220×10^{-1}	2.041×10^{-1}	1.850×10^{1}	5.556×10^{-1}	4.606×10^{-1}
2.394×10^{-1}	5.663×10^{-2}	1.722×10^{-1}	1.663×10^{4}	3.333×10^{-1}	2.018×10^{-1}
6.821×10^{-4}	3.173×10^{-2}	2.161×10^{-1}	5.947×10^{1}	5.000×10^{-1}	8.743×10^{-2}
1.211×10^{-5}	9.284×10^{-1}	1.901×10^{-1}	9.291×10^{-1}	6.250×10^{-1}	3.835×10^{-2}
5.827×10^{-3}	4.107×10^{-4}	1.862×10^{-1}	4.378×10^{2}	3.000×10^{-1}	6.306×10^{-1}
1.575×10^{-1}	1.517×10^{0}	1.581×10^{-1}	1.004×10^{4}	5.714×10^{-1}	9.078×10^{-2}
1.867×10^{-5}	4.892×10^{0}	1.781×10^{-1}	1.341×10^{0}	1.000×10^{0}	8.325×10^{-4}
2.551×10^{-4}	1.467×10^{-1}	1.742×10^{-1}	1.792×10^{1}	5.000×10^{-1}	2.121×10^{-1}
5.355×10^{-3}	1.926×10^{-2}	1.882×10^{-1}	4.065×10^{2}	4.444×10^{-1}	2.469×10^{0}
1.922×10^{-4}	6.272×10^{-1}	1.601×10^{-1}	1.242×10^{1}	5.714×10^{-1}	8.362×10^{-3}
7.507×10^{-2}	4.999×10^{-3}	2.002×10^{-1}	6.062×10^{3}	4.000×10^{-1}	1.386×10^{0}
9.612×10^{-2}	1.089×10^{-2}	1.842×10^{-1}	7.141×10^{3}	3.000×10^{-1}	9.889×10^{-1}
1.376×10^{-4}	5.399×10^{0}	1.741×10^{-1}	9.658×10^{0}	7.143×10^{-1}	9.915×10^{-4}

References

Zuend, A. and Seinfeld, J. H.: Modeling the gas–particle partitioning of secondary organic aerosol: the importance of liquid–liquid phase separation, Atmos. Chem. Phys., 12, 3857–3882, https://doi.org/10.5194/acp-12-3857-2012, 2012.